



OPEN

Estimating liver cirrhosis severity with extracellular volume fraction by spectral CT

Hong Zhang^{1,4}, Ee Hao^{2,4}, Dongqin Xia^{3,4}, Mingyue Ma¹, Jiayu Wu¹, Tongchi Liu¹, Ming Gao¹ & Xiaoping Wu¹✉

To investigate the diagnostic value of spectral CT in calculating extracellular volume fraction (ECV) for assessing the severity of liver cirrhosis. This retrospective study enrolled 172 participants, including 127 patients diagnosed with liver cirrhosis and 45 matched controls, all of whom underwent spectral CT hepatic enhancement imaging. Disease severity stratification was performed using the Child-Pugh classification system. ECV values were derived from the iodine density map during the delayed phase. These ECV values were then compared across the control group and subclassified cirrhosis groups (Child-Pugh classes A–C). Furthermore, a correlation analysis was performed to assess the relationship between ECV values and Child-Pugh scores in liver cirrhosis. Receiver operating characteristic (ROC) curves were constructed to evaluate the diagnostic performance of ECV values and MELD-Na in the Child-Pugh classification of liver cirrhosis. The ECV values were 25.49 ± 3.15 , 29.73 ± 3.20 , 35.64 ± 3.15 , and 45.30 ± 5.16 for the control, Child-Pugh A, Child-Pugh B, and Child-Pugh C group, respectively, demonstrating significant intergroup differences ($F = 184.67$, $P < 0.001$). A strong positive correlation was observed between ECV and Child-Pugh liver function classification ($r = 0.791$, $P < 0.001$). The diagnostic performance of ECV for differentiating between Child-Pugh classes A and B (AUC: 0.901), B and C (AUC: 0.966) was higher compared to the MELD-Na score (AUC: 0.772 and 0.868) ($P < 0.05$, respectively). Multivariate analyses showed that ECV was an independent factor for cirrhosis (OR 1.610, $P < 0.001$). ECV values measured using spectral CT can serve as a noninvasive biomarker for assessing the severity of liver cirrhosis.

Keywords Spectral CT, Extracellular volume, Liver cirrhosis, Child-Pugh classification, Iodine density

The etiological factors and epidemiological patterns of chronic liver diseases exhibit significant global variations. As the disease advances, it triggers a pathogenic cascade beginning with hepatic fibrosis, progressing to irreversible cirrhosis, and culminating in hepatocellular carcinoma (HCC). In recent years, the incidence rate of cirrhosis has been increasing, posing a serious burden on society and patients^{1,2}. Cirrhosis is characterized by severe scarring, structural distortion, and functional failure of liver tissue due to collagen deposition, accompanied by life-threatening complications such as portal hypertension, variceal bleeding, peritonitis, ascites, and hepatic encephalopathy³. Therefore, cirrhosis is currently the 10th leading cause of death in Africa; 9th leading cause in SE Asia and Europe; and the 5th leading cause of death in the Eastern Mediterranean². Accurate assessment of the severity of cirrhosis is of great significance for patient treatment, prognosis, and overall mortality risk assessment⁴.

Currently, various scoring methods for evaluating liver fibrosis and cirrhosis have been developed clinically based on laboratory tests⁵. However, the most widely accepted and effective scoring system in clinical practice is still the Child-Pugh score⁶. Although imagological examination also plays an important role in the prognosis assessment of cirrhosis patients, most of them are based on morphological studies, including assessments of liver size, smoothness of the liver capsule, and widening of liver fissures. These methods cannot quantify the severity of liver fibrosis and cirrhosis. Currently, ultrasound elastography is a convenient, rapid, and relatively accurate technique for assessing liver fibrosis^{7,8}. However, its clinical application is influenced by various factors (such as inflammation, cholestasis, and metabolic status), and its diagnostic accuracy is limited in specific patient populations (e.g., those with obesity, ascites, scars in the right upper abdomen, or narrow intercostal

¹Department of Radiology, Affiliated Xi'an Central Hospital of Xi'an Jiaotong University, No. 161, Xiwu Road, Xincheng District, Xi'an 710003, Shaanxi, China. ²Department of Sixth Outpatient, Xijing 986 Hospital, Xi'an 710054, China. ³Department of Ultrasound, Affiliated Xi'an Central Hospital of Xi'an Jiaotong University, Xi'an 710003, China.

⁴Hong Zhang, Ee Hao and Dongqin Xia contributed equally to this work. ✉email: szping518@163.com

spaces). Magnetic resonance elastography (MRE) is a novel non-invasive diagnostic method for liver fibrosis and cirrhosis, offering high accuracy in determining the severity of these conditions^{9,10}. However, due to its longer examination time, higher equipment requirements, and limited availability in primary care hospitals, its widespread adoption is challenging. Additionally, chronic liver diseases are often accompanied by hepatic iron deposition, and excessive iron accumulation can lead to magnetic field inhomogeneity and accelerated proton dephasing, which may also affect the accuracy of magnetic resonance elastography¹¹.

Extracellular volume fraction (ECV) is the sum of the extracellular-extravascular space fraction and the intravascular space fraction, serving as a quantifiable marker of the extracellular matrix. Chronic liver injury activates hepatic stellate cells, resulting in abnormal deposition of extracellular matrix components (collagen, fibronectin, etc.). Non-cellular components such as collagen occupy hepatic tissue space, increasing the proportion of extracellular gaps and elevating ECV¹². ECV directly measures the volumetric proportion of the extracellular matrix via CT/MRI, reflecting the core pathological alteration in liver fibrosis—excessive extracellular matrix deposition—with fewer confounding factors, higher accuracy, and the ability to detect early-stage cirrhosis¹³. ECV does not rely on subjective parameters (e.g., ascites/encephalopathy in the Child-Pugh score), effectively reducing assessment bias. Blood-based biochemical indices such as APRI (AST-to-Platelet Ratio Index), FIB-4 (Fibrosis-4 Index), and ALBI (Albumin-Bilirubin Index) only indirectly reflect fibrosis, the specificity is diminished by influences from inflammation and medications. Furthermore, serological indices are susceptible to confounding effects from composite indicators, while ECV overcomes the limitations of conventional serological markers and emerges as the sole independent determinant influencing the histological staging of liver fibrosis¹⁴. Relevant studies confirm the diagnostic performance of ECV superior to serological tests like APRI and FIB-4^{15,16}. However, there is limited research reporting on the assessment of liver cirrhosis severity staging through ECV measurements using spectral CT. Building on this research background, we hypothesize that ECV will exhibit similar advantages in grading cirrhosis severity. This study aims to provide a noninvasive biomarker for assessing cirrhosis severity. This approach integrates seamlessly with conventional imaging, advancing precision-driven management of liver diseases.

Materials and methods

Patients

We selected 127 patients who underwent spectral CT abdominal contrast-enhanced scans in our department from October 2023 to January 2025 and were clinically and pathologically diagnosed with cirrhosis. At the same time, 45 normal controls matched in gender and age were selected. The normal control group comprised three distinct cohorts: (1) asymptomatic individuals undergoing routine health check-ups; (2) patients presenting with digestive symptoms (e.g., dyspepsia, abdominal pain, or bloating); (3) subjects referred for contrast-enhanced abdominal CT scans due to incidental findings of abnormal imaging characteristics (e.g., atypical density/signal intensities) in non-hepatic abdominal organs.

General information and laboratory test results of all enrolled cases were collected, including hematocrit, platelet, prothrombin time (PT), bilirubin, albumin, aspartate aminotransferase (AST), alanine aminotransferase (ALT), and serum sodium concentration. The case group of cirrhotic patients was divided into three groups based on Child-Pugh severity of cirrhosis: Child-Pugh A, Child-Pugh B, and Child-Pugh C.

Inclusion criteria

(1) Clinically and pathologically diagnosed with cirrhosis; (2) Possess complete general information, imaging, and laboratory examination data.

Exclusion criteria

(1) Presence of liver neoplastic lesions; (2) Previous history of other malignant tumors; (3) Recent history of blood transfusion or liver trauma. (4) The CT image quality is poor, making accurate measurements unfeasible.

Normal controls inclusion criteria

(1) All laboratory liver function indicators are within normal ranges; (2) No neoplastic lesions are present in the liver. (3) There is no history of other malignant tumors. (4) No history of liver trauma or recent blood transfusion. 4. The CT image quality meets the standards required for accurate measurements.

Normal controls exclusion criteria

Contrast-enhanced upper abdominal CT revealed suspected malignant neoplastic lesions in the liver and/or other abdominal organs, or demonstrated lesions with indeterminate characteristics requiring further diagnostic evaluation.

CT examination

A triphasic contrast-enhanced scan of the liver was conducted using Philips 256-slice spectral CT, employing an automatic tracking method for blood flow detection. The diaphragm-level abdominal aorta was set as the detection plane, with a trigger threshold of 150 Hounsfield Unit (HU). Images were acquired at 8 s, 40 s, and 180 s after reaching the threshold, representing the hepatic arterial phase, portal venous phase, and delayed phase, respectively. The contrast agent used was iopromide (370 mg/ml), with a general dose of 70–90 ml (1.2 ml/kg) and an injection rate of 3 ml/s. The scanning parameters were as follows: tube voltage, 120 kV; tube current, 137 mAs, helical pitch, 0.9, slice thickness, 1.5 mm; slice interval, 1.5 mm; FOV, 320 mm. The spectral image data (spectral-based imaging, SBI) obtained after scanning was uploaded to a workstation. Although there is no definitive conclusion regarding the optimal delayed phase timing for liver imaging, based on previous related studies^{17–19}, we have chosen 180 s as the delayed phase timing for the liver.

Image post-processing and data measurement

SBI data was processed by a Philips IntelliSpace Portal V12.0 workstation. We selected the liver enhancement delay 180s image and utilized the built-in Multiphase Analysis software within the workstation to calculate ECV. After calibration, we avoided the liver vessels and calcifications, and on the liver's largest volume plane, we selected the caudate lobe (SI), the upper segment of left lateral lobe (SII), the lower segment of left lateral lobe (SIII), left medial lobe (SIV), lower segment of right anterior lobe (SV), lower segment of right posterior lobe (SVI), upper segment of right posterior lobe (SVII) and upper segment of right anterior lobe (SVIII) to draw regions of interest (ROIs) with an area of approximately 100mm² for measurement. The average ECV of the eight liver segments was taken as the liver's ECV value, as shown in (Fig. 1). The measurements were performed by two senior attending physicians, and the average value was taken as the final measurement result.

Statistical analysis

Data were entered bilaterally into Excel software, and processed using Prism 5.0 (GraphPad Software) and SPSS Statistics (Version 26, IBM). Measurement data were presented as mean \pm standard deviation, while count data were expressed as percentages (%). All data underwent normality and homogeneity of variance tests. If the data followed a normal distribution, t-tests were used for comparisons between two groups, and one-way ANOVA was applied for comparisons among multiple groups. If the data did not follow a normal distribution, the rank sum test was used. Correlation between data was analyzed using Pearson or Spearman correlation, and ROC curve analysis was used to predict the highest sensitivity and specificity and determine the optimal cutoff value. Logistic regression was used to determine independent factors for the diagnosis of cirrhosis, A p-value < 0.05 was considered statistically significant.

Results

Cohort characteristics and laboratory test

There were 58 cases in the Child-Pugh A group (36 males and 22 females), 47 cases in the Child-Pugh B group (29 males and 18 females), 22 cases in the Child-Pugh C group (14 males and 8 females), and 35 cases in the control group (19 males and 16 females). In the cirrhosis group, there were 65 cases of hepatitis B-related liver disease, 25 cases of hepatitis C-related liver disease, 2 cases of alcoholic liver disease, 6 cases of autoimmune liver disease, 1 case of Budd-Chiari syndrome, and 28 cases of cirrhosis of unknown etiology. PT, INR, bilirubin, AST, ALT, albumin, platelet, albumin-bilirubin (ALBI), and modified end-stage liver disease with the incorporation of sodium (MELD-Na) exhibited statistical differences across all groups ($P < 0.001$). Detailed data regarding age, gender, laboratory tests, and CT-measured ECV values for different subgroups are outlined in (Table 1).

Comparison of ECV values among Child-Pugh groups of liver cirrhosis

The ECV value of the control group was 25.49 ± 3.15 , whereas the ECV values for the Child-Pugh A, B, and C groups of cirrhosis were 29.73 ± 3.20 , 35.64 ± 3.15 and 45.30 ± 5.16 , respectively. One-way ANOVA analysis indicated statistically significant differences in ECV among the groups ($F = 184.67$, $P < 0.001$), (Fig. 2).

Correlation between ECV value and Child-Pugh classification of liver cirrhosis

A correlation analysis was conducted between the ECV value with the Child-Pugh score. The ECV value demonstrated a significant positive correlation with the Child-Pugh score for cirrhosis ($r = 0.791$, $p < 0.001$). The results indicated that as the severity of cirrhosis increased, the ECV value tended to rise (Fig. 3).

Diagnostic efficacy of ECV value in assessing the severity of liver cirrhosis

The receiver operating characteristic (ROC) curve shows the area under the curve (AUC) of the ECV value for diagnosing the control group and cirrhosis group was 0.911 (95% CI 0.858–0.949). Using a cutoff value of 29.46, the best discrimination between non-cirrhosis and cirrhosis was achieved, with sensitivity and specificity

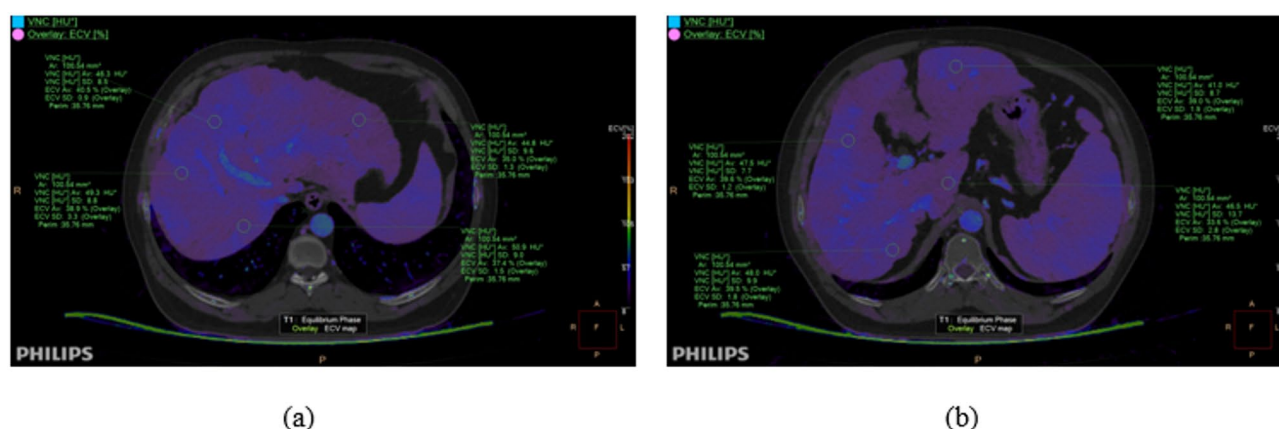


Fig. 1. ECV measurement based on Multiphase Analysis software in Philips IntelliSpace Portal V12.0 workstation. (a) ROIs drawn in the SII, SIV, SVII, and SVIII; (b) ROIs drawn in the SI, SIII, SV, and SVI.

Variable	Controls (n = 45)	Child-Pugh A (n = 58)	Child-Pugh B (n = 47)	Child-Pugh C (n = 22)	P value
Clinical parameters					
Age, years	57.27 (11.53)	58.17 (11.35)	59.38 (12.85)	57.45 (9.44)	0.833
Sex					0.880
Female, %	14 (31.1)	22 (37.9)	18 (38.3)	8 (36.4)	
Male, %	31 (68.9)	36 (62.1)	29 (61.7)	14 (63.6)	
Liver disease type					<0.001
Hepatitis B virus	–	30 (51.7)	21 (44.7)	14 (63.6)	
Hepatitis C virus	–	12 (20.7)	7 (14.9)	6 (27.3)	
Autoimmune hepatitis	–	2 (3.4)	3 (6.4)	1 (4.5)	
Budd-Chiari syndrome	–	0 (0.0)	1 (2.1)	0 (0.0)	
Alcoholic hepatitis	–	1 (1.7)	1 (2.1)	0 (0.0)	
Unknown	–	13 (22.4)	14 (29.8)	1 (4.5)	
Laboratory parameters					
Hematocrit value (%)	40.84 (4.17)*	36.64 (7.68)*	32.77 (7.93)*	30.31 (7.86)*	<0.001
PT (s)	10.38 (1.34)*	12.06 (1.88)*	14.00 (1.85)*	17.42 (3.14)*	<0.001
INR	0.88 (0.08)*	1.02 (0.14)*	1.17 (0.15)*	1.48 (0.33)*	<0.001
Bilirubin (umol/l)	13.38 (5.43)*	22.75 (11.50)*	31.48 (16.47)*	89.37 (106.35)*	<0.001
Albumin (g/l)	42.82 (3.14)*	39.64 (4.62)*	33.79 (5.17)*	28.58 (3.15)*	<0.001
AST (U/l)	20.02 (5.75)*	40.97 (51.61)*	45.57 (36.02)*	134.82 (211.67)*	<0.001
ALT (U/l)	17.87 (8.16)*	30.29 (23.24)*	33.77 (30.97)*	98.59 (149.32)*	<0.001
Na (mmol/l)	140.20 (1.87)*	139.74 (2.44)*	138.06 (3.32)*	137.55 (5.44)*	<0.001
Platelet (10 ⁹ /l)	216.91 (59.00)*	106.22 (54.42)*	99.37 (74.77)*	109.14 (91.61)*	<0.001
Creatinine (umol/l)	62.00 (13.93)*	58.71 (13.23)*	64.14 (23.24)*	73.83 (20.31)*	0.008
Child-pugh score	5.00 (0.00)*	5.55 (0.50)*	7.62 (0.64)*	11.32 (1.55)*	<0.001
MELD_Na score	–2.90 (0.30)*	–2.51 (0.43)*	–1.92 (0.42)*	–1.25 (0.41)*	<0.001
ALBI score	–2.94 (0.30)*	–2.51 (0.43)*	–1.86 (0.37)*	–1.08 (0.37)*	<0.001
CT parameters					
ECV (%)	25.49 (3.15)*	29.73 (3.20)*	35.64 (3.15)*	45.30 (5.16)*	<0.001

Table 1. Clinical, laboratory, and CT parameters. *ECV* extracellular volume fraction, *ALBI* albumin-bilirubin, *MELD-Na* modified end-stage liver disease with the incorporation of sodium, *PT* prothrombin time, *INR* international normalized ratio, *AST* aspartate aminotransferase, *ALT* alanine aminotransferase. * $P < 0.05$, compared to the control group; # $P < 0.05$, compared to the Child-Pugh C. Continuous variables are expressed as mean \pm standard deviation. Categorical variables are expressed as numbers and percentages in parentheses.

of 76.38 and 95.56%, respectively. The AUC of the ECV value for diagnosing Child-Pugh A and Child-Pugh B stages of cirrhosis was 0.901, which was significantly higher than that of MELD-Na ($Z = 2.441$, $p = 0.015$); The AUC of the ECV value for diagnosing Child-Pugh B and Child-Pugh C stages of cirrhosis was 0.966 (95% CI 0.892–0.995), which was significantly higher than that of MELD-Na ($Z = 2.042$, $p = 0.041$). (Fig. 4; Table 2).

Analysis of risk factors for liver cirrhosis

As shown in Table 3, multivariate logistic regression analysis showed that ECV was independently associated with liver cirrhosis (OR 1.610, CI 1.219–2.125, $P < 0.001$).

Discussion

The extracellular volume fraction (ECV) is the sum of the fractions of the extravascular-extracellular space and intravascular space, reflecting the microvascular density and the degree of matrix fibrosis. Based on this principle, ECV has initially been extensively utilized in the assessment of myocardial fibrosis, particularly in evaluating myocardial fibrosis and myocardial lesions through magnetic resonance T1 mapping^{20,21}. Apart from its application in the assessment of myocardial fibrosis²², CT-based ECV measurement has also been employed for distinguishing between benign and malignant tumors, assessing tumor staging, evaluating treatment response, and predicting prognosis²³.

Patients with liver fibrosis and cirrhosis exhibit an increase in collagen deposition within the liver, subsequently enlarging the extracellular space. Given this pathological basis, the degree of liver fibrosis can be indirectly reflected through the quantitative measurement of liver ECV values²⁴. Methods for measuring ECV values via CT include ECV- Δ HU, which relies on CT values, and ECV-Iodine, which utilizes iodine density maps. In the context of liver ECV measurement among patients with liver fibrosis, Yoon et al. conducted a Spectral CT study and discovered that ECV-Iodine demonstrates superior diagnostic efficacy for liver fibrosis ($F \geq 2$) compared to ECV-HU²⁵. Similarly, Nagayama et al. employed dual-energy CT and observed that the correlation coefficient of ECV-Iodine is higher than that of ECV- Δ HU within the liver fibrosis group, indicating a higher

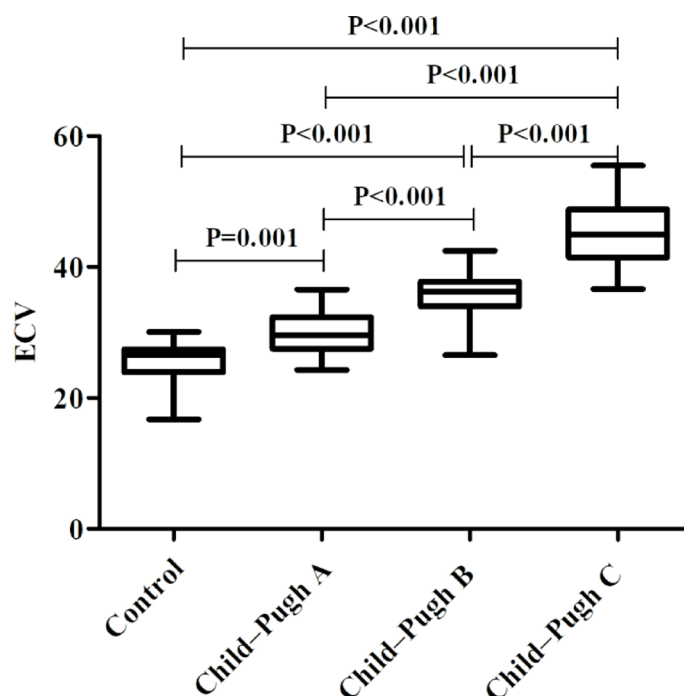


Fig. 2. One-way ANOVA test of extracellular volume fraction in the control group and cirrhosis groups.

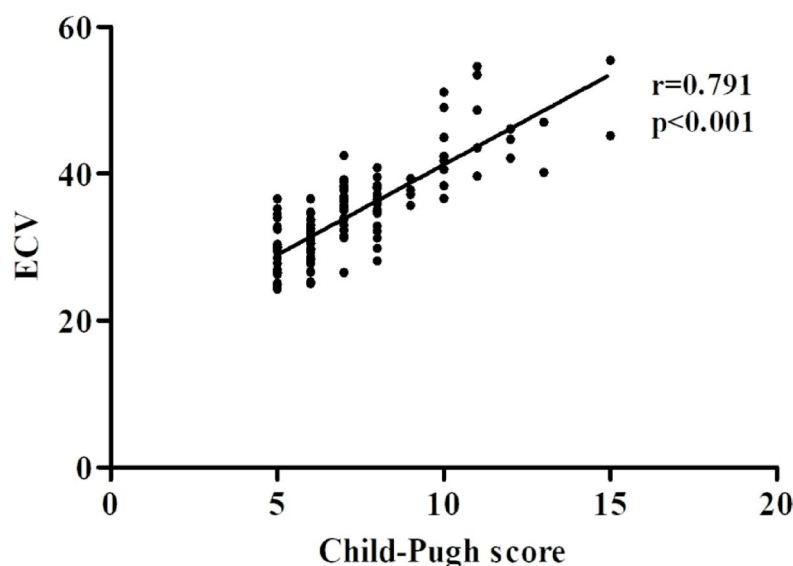


Fig. 3. Correlations of ECV with Child-Pugh score in liver cirrhosis.

degree of reliability and credibility for ECV-Iodine in assessing liver fibrosis²⁶. Consequently, this study employs Spectral CT to calculate liver ECV values based on iodine density maps. Currently, the majority of domestic and international literature primarily focuses on evaluating the degree of liver fibrosis in the application of ECV, with limited reports on cirrhosis research. However, since the liver fibrosis stage has already progressed in cirrhosis patients, merely assessing the fibrosis stage appears insufficient to draw conclusive insights into the severity of liver function. ECV may hold promising potential in the management of liver diseases. Recently, scholars have demonstrated that the measurement of ECV values utilizing T1 mapping technology can effectively evaluate the grading of liver function in cirrhosis patients^{27,28}. Xu et al. further discovered through dual-energy CT that ECV values hold predictive potential for short-term disease progression in patients with acute decompensated hepatitis B cirrhosis²⁹. Hong et al. discovered ECV serves as an independent predictor of high-risk esophageal varices (HRV) in cirrhosis³⁰. The combination of ECV quantification and platelet count demonstrated superior diagnostic performance compared to the conventional CT imaging plus platelet count standard in ruling out

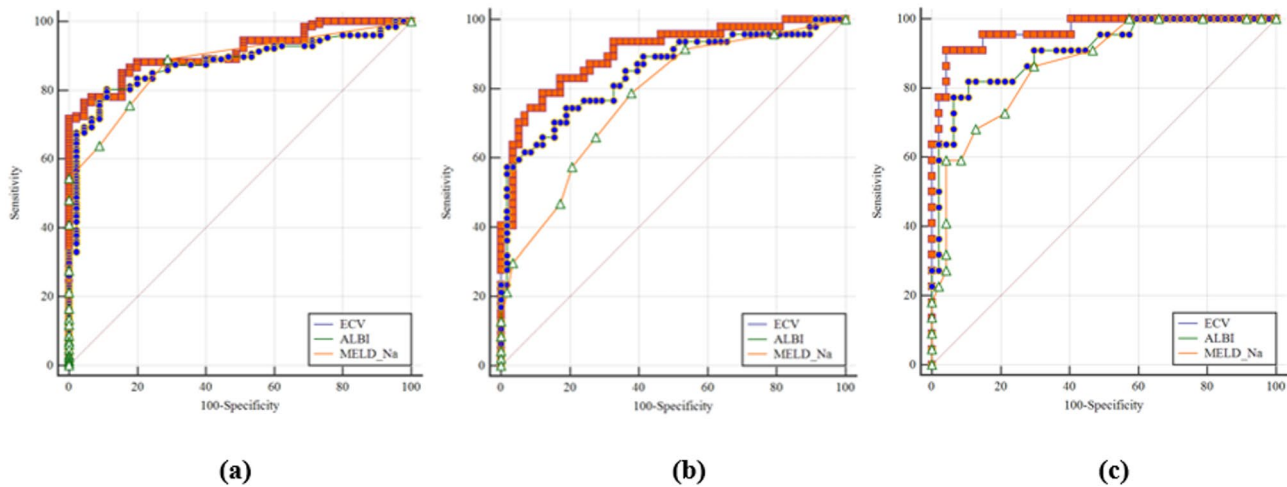


Fig. 4. Graphs show receiver operating characteristic curves of ECV as well as clinical scores of liver disease severity for differentiation between Controls and cirrhosis (a), Child-Pugh A and B classes (b), and Child-Pugh B and C classes (c).

		AUC	Cutoff value	Sensitivity (%)	Specificity (%)	PPV (%)	NPV (%)	Youden
Control vs. cirrhosis	ECV	0.911 (0.858 to 0.949)	29.46	76.38 (68.0–83.5)	95.56 (84.9–99.5)	98.0 (92.9–99.8)	58.9 (46.8–70.3)	0.719
	ALBI	0.878 (0.819 to 0.923)	-2.65	80.31 (72.3–86.8)	88.89 (75.9–96.3)	95.3 (89.4–98.5)	61.5 (48.6–73.3)	0.692
	MELD_Na	0.868 (0.810 to 0.911)	6	88.98 (82.2–93.8)	71.11 (55.7–83.6)	89.7 (83.0–94.4)	69.6 (54.2–82.3)	0.601
Child-Pugh A vs. B	ECV [#]	0.901 (0.827 to 0.951)	33.72	78.72 (64.3–89.3)	87.93 (76.7–95.0)	84.1 (69.9–93.4)	83.6 (71.9–91.8)	0.667
	ALBI	0.847 (0.764 to 0.910)	-1.87	57.45 (42.2–71.7)	98.28 (90.8–100.0)	96.4 (81.7–99.9)	74.0 (62.8–83.4)	0.557
	MELD_Na	0.772 (0.680 to 0.848)	8	78.72 (64.3–89.3)	62.07 (48.4–74.5)	62.7 (49.1–75.0)	78.3 (63.6–89.1)	0.408
Child-Pugh B vs. C	ECV [#]	0.966 (0.892 to 0.995)	39.53	90.91 (70.8–98.9)	95.74 (85.5–99.5)	90.9 (70.8–98.9)	95.7 (85.5–99.5)	0.867
	ALBI	0.906 (0.811 to 0.963)	-1.5	81.82 (59.7–94.8)	89.36 (76.9–96.5)	78.3 (56.3–92.5)	91.3 (79.2–97.6)	0.712
	MELD_Na	0.868 (0.764 to 0.937)	12	86.36 (65.1–97.1)	70.21 (55.1–82.7)	57.6 (39.2–74.5)	91.7 (77.5–98.2)	0.566

Table 2. Diagnostic efficacy of ECV, ALBI, and MELD-Na for controls and subclassified cirrhosis groups. ECV extracellular volume fraction, ALBI albumin-bilirubin, MELD-Na model of end-stage liver disease with the incorporation of sodium. [#]Represents the diagnostic efficacy is statistically significant ($p<0.05$).

Variable	OR	95% CI	p-value
ECV	1.610	1.219–2.125	0.001
Sex	0.642	0.164–2.512	0.524
Age	1.019	0.958–1.085	0.543
Prothrombin time	1.588	0.961–2.627	0.071
Bilirubin	1.087	0.943–1.253	0.251
Albumin	1.018	0.832–1.246	0.863
AST	1.164	1.021–1.328	0.024
ALT	0.995	0.911–1.087	0.906
Creatinine	0.975	0.918–1.035	0.407
MELD-Na	1.344	0.655–2.758	0.420

Table 3. Logistic regression analysis of liver cirrhosis patients versus controls.

HRV. This integrated approach may accurately identify high-risk varices while potentially reducing unnecessary endoscopic examinations. Related studies demonstrate that ECV had a higher diagnostic efficacy than serum fibrosis markers in predicting HCC and post-HCC resection liver failure risk^{17,31}. This study revealed that the ECV values for the normal control group, Child-Pugh A group, Child-Pugh B group, and Child-Pugh C group were 25.49 ± 3.15 , 29.73 ± 3.20 , 35.64 ± 3.15 , and 45.30 ± 5.16 respectively. Notably, there was a statistically significant difference across all groups ($F=184.67$, $P<0.001$), which aligns closely with the findings of Mesrobian et al., who examined the correlation between magnetic resonance ECV

values and the severity of liver cirrhosis³². Furthermore, Wang et al. observed a significant positive correlation between liver ECV values measured using spectral CT and liver function classification ($r=0.85$, $P<0.05$)³³. Similarly, our study demonstrated a significant positive correlation between ECV and liver function Child-Pugh classification based on spectral CT measurements ($r=0.791$, $P<0.001$). This suggests that as the severity of liver cirrhosis progresses, there is a continuous increase in the synthesis and deposition of extracellular matrix proteins, leading to the expansion of the extracellular space and consequently, elevated ECV values. Multivariate analyses showed that ECV was the factor independently associated with cirrhosis (OR=1.610, $P<0.001$), and the analysis of the ROC showed ECV value for diagnosing the control group and cirrhosis group was 0.911 (95% CI 0.858–0.949), suggesting that ECV can be used as a biomarker for early identification of cirrhosis. Our study revealed that the area under the curve (AUC) for ECV in discriminating between Child-Pugh A and B, as well as Child-Pugh B and C, exceeded that of MELD-Na. Notably, CT-based ECV measurement exhibited superior diagnostic efficacy compared to MELD-Na derived from laboratory tests. This superiority can be attributed to several factors. Firstly, MELD-Na incorporates diverse laboratory markers in assessing liver function, which may be influenced by lesions outside the liver and comorbidities unrelated to liver disease, thereby compromising their specificity. Secondly, utilized in calculating ECV are directly sourced from the liver parenchyma and normalized with respect to hematocrit, potentially leading to more pure and accurate predictions.

This study has several limitations. First, the retrospective design is inherently subject to selection bias. Second, the relatively small sample size, particularly the limited number of Child-Pugh C cases, may introduce sampling bias and limit the generalizability and statistical power of the findings. Third, due to practical constraints, we opted to inject the contrast agent 180 s after the delay period. However, further investigation is warranted to determine whether a longer delay period would yield different results in ECV value measurement. Lastly, while this study encompassed various types of cirrhosis stemming from diverse etiologies, the number of cases attributed to etiologies other than hepatitis B and hepatitis C was insufficient. Consequently, no further exploration was conducted to assess potential differences in ECV values among cirrhosis cases with different etiologies. Future studies should aim to expand the sample size, particularly for Child-Pugh C cases and non-hepatitis cirrhosis cases.

Conclusion

In this study, the measurement of ECV values utilizing spectral CT iodine concentration maps revealed significant inter-group disparities between the control group and various Child-Pugh cirrhosis groups. Notably, a positive correlation was observed between ECV values and Child-Pugh scores. Furthermore, in the ROC diagnostic performance evaluation, the ECV measurement possess relative advantages. Preliminary evidence suggests that ECV measurements may provide distinct advantages in specific clinical contexts. Our findings indicate that ECV values could serve as potential non-invasive biomarkers for cirrhosis severity grading, though their clinical utility requires validation in larger prospective cohorts with longitudinal outcomes.

Data availability

All relevant data for this study are included within the manuscript. The raw data that support the findings of this study are available from the corresponding author upon reasonable request.

Received: 16 February 2025; Accepted: 22 May 2025

Published online: 26 May 2025

References

- Ginès, P. et al. Liver cirrhosis. *Lancet* **398** (10308), 1359–1376 (2021).
- Devarbhavi, H. et al. Global burden of liver disease: 2023 update. *J. Hepatol.* **79** (2), 516–537 (2023).
- Chinese Society of Gastroenterology, Chinese Medical Association. Chinese consensus on the management of liver cirrhosis. *J. Dig. Dis.* **25** (6), 332–352 (2024).
- Qi, X., Arora, A., Tang, S., Mancuso, A. & Romeiro, F. G. Prognostic assessment and management of liver cirrhosis. *Biomed. Res. Int.* **2017**, 5326898 (2017).
- Smith, A., Baumgartner, K. & Bositis, C. Cirrhosis: diagnosis and management. *Am. Fam. Physician.* **100** (12), 759–770 (2019).
- El Hajra, I. et al. Outcome of patients with HCC and liver dysfunction under immunotherapy: a systematic review and meta-analysis. *Hepatology* **77** (4), 1139–1149 (2023).
- Ferraioli, G. & Barr, R. G. Ultrasound liver elastography beyond liver fibrosis assessment. *World J. Gastroenterol.* **28** (24), 3413–3420 (2020).
- Fang, C., Lim, A. & Sidhu, P. S. Ultrasound-based liver elastography in the assessment of fibrosis. *Clin. Radiol.* **75** (11), 822–831 (2020).
- Ajmera, V. H. et al. Clinical utility of an increase in magnetic resonance elastography in predicting fibrosis progression in nonalcoholic fatty liver disease. *Hepatology* **71** (3), 849–860 (2020).
- Kupczyk, P. A. et al. Quantitative MRI of the liver: evaluation of extracellular volume fraction and other quantitative parameters in comparison to MR elastography for the assessment of hepatopathy. *Magn. Reson. Imaging.* **77**, 7–13 (2021).
- Wang, X. P. et al. Assessment of liver fibrosis with liver and spleen magnetic resonance elastography, serum markers in chronic liver disease. *Quant. Imaging Med. Surg.* **10** (6), 1208–1222 (2020).
- Wiese, S. et al. Fibrogenesis and inflammation contribute to the pathogenesis of cirrhotic cardiomyopathy. *Aliment. Pharmacol. Ther.* **52** (2), 340–350 (2020).
- Morita, K. et al. Noninvasive assessment of liver fibrosis by dual-layer spectral detector CT. *Eur. J. Radiol.* **136**, 109575 (2021).
- Wang, H. Q. et al. Assessing liver fibrosis in chronic hepatitis B using MR extracellular volume measurements: comparison with serum fibrosis indices. *Magn. Reson. Imaging.* **59**, 39–45 (2019).
- Kokubo, R. et al. Comparison of liver fibrosis and function indices with extracellular volume using dual-energy CT: A retrospective study. *Curr. Med. Imaging.* **18** (11), 1180–1185 (2022).
- Obmann, V. C. et al. MRI extracellular volume fraction in liver fibrosis—A comparison of different time points and blood pool measurements. *J. Magn. Reson. Imaging.* **60** (4), 1678–1688 (2024).

17. Ozaki, K. et al. Liver fibrosis estimated using extracellular volume fraction obtained from dual-energy CT as a risk factor for hepatocellular carcinoma after sustained virologic response: A preliminary case-control study. *Eur. J. Radiol.* **168**, 111112 (2023).
18. Huang, X. et al. Extracellular volume fraction of liver and pancreas using spectral CT in hypertensive patients: A comparative study. *J. Xray Sci. Technol.* **32** (6), 1351–1362 (2024).
19. Cicero, G. et al. Dual-energy CT quantification of fractional extracellular space in cirrhotic patients: comparison between early and delayed equilibrium phases and correlation with oesophageal varices. *Radiol. Med.* **126** (6), 761–767 (2021).
20. Kitkungvan, D. et al. Extracellular volume in primary mitral regurgitation. *JACC Cardiovasc. Imaging.* **14** (6), 1146–1160 (2021).
21. Porcari, A. et al. Redefining cardiac involvement and targets of treatment in systemic Immunoglobulin AL amyloidosis. *JAMA Cardiol.* **21**, e242555 (2024).
22. Kato, S. et al. Clinical utility of computed tomography-derived myocardial extracellular volume fraction: A systematic review and meta-analysis. *JACC Cardiovasc. Imaging.* **17** (5), 516–528 (2024).
23. Fujita, N. et al. Extracellular volume fraction determined by dual-layer spectral detector CT: possible role in predicting the efficacy of preoperative neoadjuvant chemotherapy in pancreatic ductal adenocarcinoma. *Eur. J. Radiol.* **162**, 110756 (2023).
24. Ozaki, K. et al. Extracellular volume fraction obtained by dual-energy CT depicting the etiological differences of liver fibrosis. *Abdom. Radiol. (NY)*. **48** (6), 1975–1986 (2023).
25. Yoon, J. H. et al. Hepatic fibrosis grading with extracellular volume fraction from iodine mapping in spectral liver CT. *Eur. J. Radiol.* **137**, 109604 (2021).
26. Nagayama, Y. et al. Liver fibrosis assessment with multiphasic dual-energy CT: diagnostic performance of iodine uptake parameters. *Eur. Radiol.* **31** (11), 8823–8824 (2021).
27. Xu, H. et al. Research on the evaluation of the liver function grading for the patients with hepatitis B cirrhosis using T1 mapping based extracellular volume fraction. *Chin. J. Magn. Reson. Imaging.* **14** (05), 132–138 (2023).
28. Hoffman, D. H. et al. T1 mapping, T2 mapping and MR elastography of the liver for detection and staging of liver fibrosis. *Abdom. Radiol. (NY)*. **45** (3), 692–700 (2020).
29. Xu, Y. et al. Dual-energy CT quantification of extracellular liver volume predicts short-term disease progression in patients with hepatitis B liver cirrhosis-acute decompensation. *Insights Imaging.* **14** (1), 51 (2023).
30. Hong, S. et al. Quantification of liver extracellular volume using dual-energy CT for ruling out high-risk varices in cirrhosis. *Eur. J. Radiol.* **148**, 110151 (2022).
31. Peng, Y. et al. CT-derived extracellular volume and liver volumetry can predict posthepatectomy liver failure in hepatocellular carcinoma. *Insights Imaging.* **14** (1), 145 (2023).
32. Mesrobian, N. et al. Assessment of liver cirrhosis severity with extracellular volume fraction MRI. *Sci. Rep.* **12** (1), 9422 (2022).
33. Wang, Y. et al. The application value of spectral CT in liver function classification of liver cirrhosis. *J. Chin. Clin. Med. Imaging.* **33** (11), 779–783 (2022).

Author contributions

All authors had full access to all the data in the study and take responsibility for the integrity of the data and the accuracy of the data analysis. Software, E.H. and J.W.; Investigation, T.L.; Formal Analysis, J.W. and E.H.; Resources, X.W. and M.M.; Data curation, M.G.; Writing - Original Draft, H.Z. and D.X.; Writing - Review & Editing, X.W.; Funding Acquisition, H.Z. and X.W.

Funding

This work was supported by grants from the Xi'an Science and Technology Program Project (No. 24YXYJ0073, NO. 23YXYJ0004, NO. 24YXYJ0041).

Declarations

Competing interests

The authors declare no competing interests.

Ethical approval

This retrospective study was conducted in accordance with the Declaration of Helsinki and was approved by the ethics committee of Xi'an Central Hospital (Approval no. LW-2025-012). The requirement for written informed consent was waived by the ethics committee due to the anonymized nature of the historical data and the observational design of this study.

Additional information

Correspondence and requests for materials should be addressed to X.W.

Reprints and permissions information is available at www.nature.com/reprints.

Publisher's note Springer Nature remains neutral with regard to jurisdictional claims in published maps and institutional affiliations.

Open Access This article is licensed under a Creative Commons Attribution-NonCommercial-NoDerivatives 4.0 International License, which permits any non-commercial use, sharing, distribution and reproduction in any medium or format, as long as you give appropriate credit to the original author(s) and the source, provide a link to the Creative Commons licence, and indicate if you modified the licensed material. You do not have permission under this licence to share adapted material derived from this article or parts of it. The images or other third party material in this article are included in the article's Creative Commons licence, unless indicated otherwise in a credit line to the material. If material is not included in the article's Creative Commons licence and your intended use is not permitted by statutory regulation or exceeds the permitted use, you will need to obtain permission directly from the copyright holder. To view a copy of this licence, visit <http://creativecommons.org/licenses/by-nc-nd/4.0/>.

© The Author(s) 2025